



TECHNICAL REPORTS: METHODS

10.1029/2018EA000442

Key Points:

- Esh3D evaluates Eshelby solution for ellipsoidal inclusions in full or half-space
- Half space Eshelby solution is obtained seminumerically by traction cancellation
- The half-space solution allows nonplanar surface

Correspondence to:

C. Meng,
cmeng@mit.edu

Citation:

Meng, C. (2019). Esh3D, an analytical and numerical hybrid code for full space and half-space Eshelby's inclusion problems. *Earth and Space Science*, 6, 505–514. <https://doi.org/10.1029/2018EA000442>

Received 9 AUG 2018

Accepted 10 FEB 2019

Accepted article online 20 FEB 2019

Published online 2 MAR 2019

Esh3D, an Analytical and Numerical Hybrid Code for Full Space and Half-Space Eshelby's Inclusion Problems

C. Meng¹

¹Department of Earth Atmosphere and Planetary Sciences, Massachusetts Institute of Technology, Cambridge, MA, USA

Abstract I present an open source code Esh3D that evaluates the quasi-static elastic displacement and stress fields perturbed by ellipsoidal inclusions, known as the Eshelby solution. The improvement over my previous work includes obtaining solutions in half-space by numerically canceling the traction to stage a free surface. The discrete numerical domain allows nonplanar surface. I first briefly introduce the ellipsoidal inclusion problem and solution evaluation. Then, I describe the traction cancellation method in forming the half-space solutions. Next, I emulate a planar fault with a low aspect ratio ellipsoid and compare the half-space solution against the well-known Okada solution for flat and topographic surfaces. Finally, I provide comparisons between the full space and half-space solutions to illustrate the free surface effects on the displacement and stress fields.

Plain Language Summary In a number of geophysical applications, our code presented in Meng et al. (2012, <https://doi.org/10.1016/j.cageo.2011.07.008>) is adopted. Among those, people sometimes use the code to fit surface deformation/strain data. However, the original code is for full space without considering the free surface. Now I extend the code to cover both the full space and half surface cases. In the last figure, I show that the free surface effect cannot be neglected even at depth of 4 km.

1. Introduction

The Eshelby's inclusion problem describes the perturbed elastic field in an infinite homogeneous elastic body as a result of the presence of an ellipsoidal inclusion. Eshelby (1957, 1959, 1961), in his celebrated work to solve this problem, treats an infinite homogeneous elastic medium with three steps of operations. First, remove an ellipsoidal inclusion from the host matrix, and impose a uniform inelastic transformation, known as *eigenstrain* to this inclusion. Finally, glue the inclusion back in the host without any surface slip. Because of the transformation, the interior and exterior of the inclusion will be subject to strains that are different than in the original state. Eshelby proves that the (constrained) interior strain will be uniform and have linear relationship with the eigen (inelastic) strain by

$$\epsilon_{ij} = S_{ijkl} \epsilon_{kl}^*, \quad (1)$$

where ϵ_{kl}^* is the eigenstrain and S_{ijkl} is named *Eshelby tensor*. To evaluate this tensor for a triaxial ellipsoid, one needs to compute a set of rank 1 and 2 integrals, commonly denoted by I_s .

Mura (1987, 22.8–22.13) provides the formulation for the exterior elastic strain,

$$\epsilon_{ij}(\mathbf{x}) = D_{ijkl}(\mathbf{x}) \epsilon_{kl}^*. \quad (2)$$

Unlike the constant Eshelby tensor, $D_{ijkl}(\mathbf{x})$ is a function of the evaluation location \mathbf{x} relative to the ellipsoid center. This tensor consists of similar, but spatially varying, I integrals and their first- and second-order gradients.

The stress can be obtained by left multiplying the elastic strain tensors with the stiffness tensor,

$$\sigma_{ij}(\mathbf{x}) = \begin{cases} C_{ijkl}(S_{klmn} \epsilon_{mn}^* - \epsilon_{kl}^*), & \text{interior,} \\ C_{ijkl} D_{klmn}(\mathbf{x}) \epsilon_{mn}^*, & \text{exterior.} \end{cases} \quad (3)$$

For the interior stress, the inelastic strain needs to be subtracted from the total strain.

©2019. The Authors.

This is an open access article under the terms of the Creative Commons Attribution-NonCommercial-NoDerivs License, which permits use and distribution in any medium, provided the original work is properly cited, the use is non-commercial and no modifications or adaptations are made.

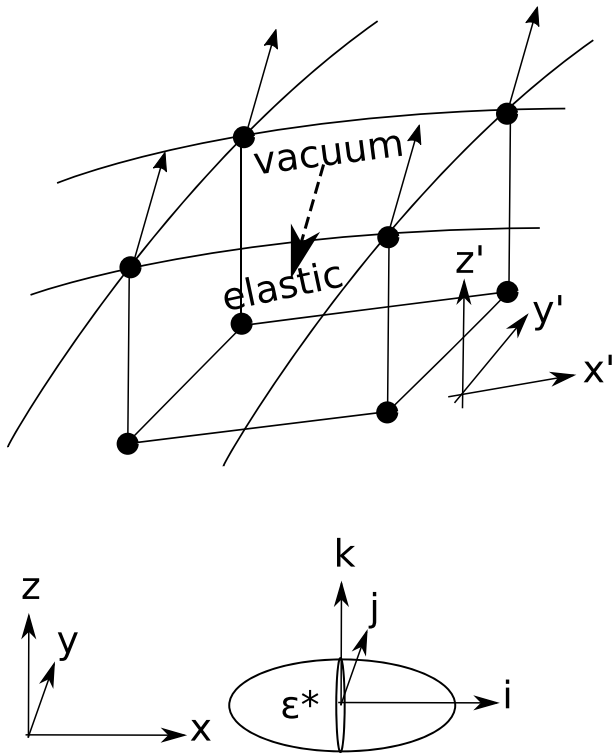


Figure 1. Schematics of numerical traction cancellation. Minimizing the objective traction, dashed arrow in Pascals, by nodal forces, solid arrows in Newtons, at the surface. The traction and nodal forces are opposite in directions but are different in quantities.

Meng et al. (2012) modify (Mura, 1987, 11.30) to obtain the displacement field

$$u_i(\mathbf{x}) = \frac{1}{8\pi(1-\nu)} \left(\psi_{,jli} \epsilon_{jl}^* - 2\nu \epsilon_{mm}^* \phi_{,i} - 4(1-\nu) \epsilon_{ii}^* \phi_{,i} \right), \quad (4)$$

where ν is Poisson's ratio and ϕ and ψ are given by integrals

$$\begin{aligned} \phi(\mathbf{x}) &= \int_{\Omega} |\mathbf{x} - \mathbf{x}'| d\mathbf{x}', \\ \psi(\mathbf{x}) &= \int_{\Omega} \frac{1}{|\mathbf{x} - \mathbf{x}'|} d\mathbf{x}', \end{aligned} \quad (5)$$

where Ω is the inclusion region. The subscript $(\cdot)_{,i}$ denotes spatial gradient in i th dimension.

Meng et al. (2012) combine (Mura, 1987, 11.40.4) with (Ferrers, 1877) to express the gradients of ϕ and ψ in equation (4) with the I integrals. Meng et al. (2012) also simplify the expressions in Mura, (1987, 11.40.1–11.40.4) with Gradshteyn and Ryzhik (1965) to express the I integrals and their gradients with a spatial variable λ and its gradients; λ is the largest root of

$$\frac{x_1^2}{a_1^2 + \lambda} + \frac{x_2^2}{a_2^2 + \lambda} + \frac{x_3^2}{a_3^2 + \lambda} = 1 \quad (6)$$

for an exterior \mathbf{x} and 0 for interior.

Reches (1998) and Healy (2009) present closed form solution with computer codes, where two of the ellipsoid's semiaxes are equal. A computer code that evaluates the true triaxial Eshelby solution has not appeared in public domain until Meng et al. (2012) present their code Esh3D (originally in Matlab™) and make it open source.

To evaluate the strain and displacement, Esh3D numerically approximates the incomplete elliptical integrals of the first and second kinds by a Matlab routine (Igor, 2005). Therefore, the full space solution is not purely analytical. To distinguish from the numerical part introduced in this study, I simply call the full space solution the analytical part.

Eshelby solution has wide application in Earth science. Rudnicki (1977, 1999) uses the solution to investigate the inception of faulting and to calculate the alteration of regional stress by inhomogeneities. Healy et al. (2006) use the solution to model the evolution of polymodal fracture patterns. Eidelman and Reches (1992) use the solution to interpret the tectonic stress state from fracture patterns in pebbles embedded in a conglomerate. Sharma and Ganti (2004) modify the original solution to simulate nanoinclusions. Katsman (2010) uses the solution to model compaction bands. Jiang (2007, 2014, 2016) extends Eshelby's formalism to allow viscous and anisotropic materials and reviews the efforts that make the solution more explicit, among which Ju and Sun (1999) provide an alternative expression for the exterior Eshelby tensor.

Esh3D has been used in a number of researches. Meng and Pollard (2014) extend the compaction band model to 3-D. Meng et al. (2013) study stress field around mixed mode fracture tip. Townsend et al. (2015) study elastic perturbation due to volcanic dike intrusion. Bedayat and Dahi Taleghani (2015) study poroelastic deformations. Guido et al. (2015) and Niu et al. (2017) study ground deformation above reservoirs. Carter et al. (2018) study fatigue crack deflections.

Above applications reflect the need for an efficient and maintainable Eshelby code. Matlab™, however, is not high performing and not freely accessible. Part of the motivation to revisit Esh3D is to translate the Matlab code to Fortran 90 for better performance and availability. The reason I choose Fortran over more popular languages is that among all the high-performing languages, only Fortran supports multidimensional array operation without third parties. To better work with various data, the model input generation and result visualization are implemented in Python.

Another, and more important, motivation of this study is to address the limitation of the original Eshelby solution that it is only for full space. In solid Earth geophysics, however, the Earth crust is better considered

Table 1
Parameters in Comparing Eshelby and Okada Solutions

Parameters	Eshelby' inclusion	Okada's fault
Geometries	$a_i = [3, 2, 10^{-3}]$ km ellipsoid	60-by-40 squares over 6 by 4 km
Elastic moduli	$E = 80$ GPa, $\nu = 0.25$	Same
Orientations	dip = $0, \pi/4$ around y axis	Same
Transformations	$\epsilon_{kk}^* = 0.1, \epsilon_{ik}^* = 0.1$	opening $\in [0, 0.194]$ m, dip slip $\in [0, 0.396]$ m
Sources	centered at $[0, 0, -15]$ km	Same
Evaluations	$x \in [-20, 20], y = 0, z = [-4, 0]$ km	Same

as an elastic half-space. Due to this reason, the code (Okada, 1985) for planar dislocations in half-space has been widely used. An obvious advantage of the Eshelby solution is that it is capable of modeling volume changes in addition to fault dislocations. Svoboda et al. (2018) also express the need for the half-space solution in studying impurity interaction. To make Esh3D more applicable in geophysics, as well as in other disciplines, I have obtained the half-space solution in a semi-analytical-numerical way. The reasons to incorporate numerical method instead of seeking analytical alternatives are stated as follows:

- From Eshelby (1957) to Meng et al. (2012), it has been a long journey to be able to evaluate the triaxial solution for full space. The analytical solution for half-space, even if exists, can be many orders more complicated.
- A numerical method is capable of modeling surface topography, which may have significant impact to the displacement and stress. This is demonstrated in section 3.2.

Incorporating with a numerical part inevitably makes the new Esh3D subject to convergence and numerical errors, as well as additional computational cost. Thanks for the discrete domain, however, Esh3D enjoys the

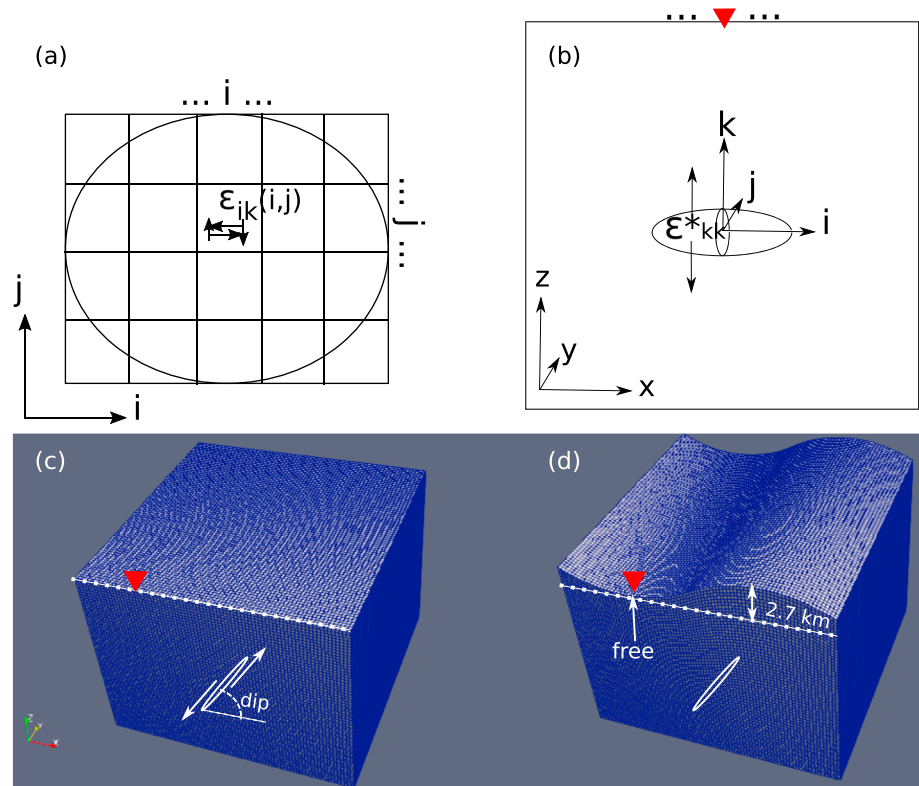


Figure 2. (a) Okada's fault made of tiles with dislocations sampled from a low-aspect Eshelby's inclusion; (b) an ellipsoidal inclusion of semiaxes (3, 2, 1) km, subject to uniaxial eigenstrain ϵ_{kk}^* , beneath a flat surface; (c) a discrete domain that contains a dip-slip ellipsoidal fault with flat top surface; (d) a domain with top surface fluctuating along the x -direction.

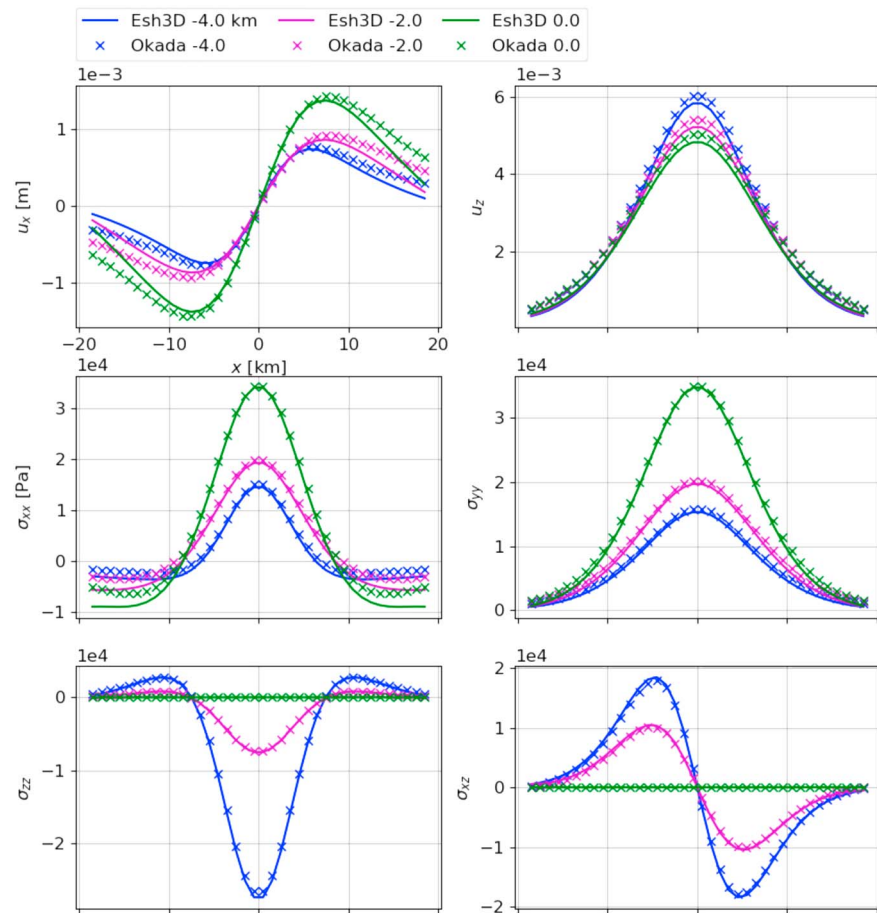


Figure 3. Displacement and stress above a zero dip and opening fault produced by Eshelby's inclusion and Okada's fault models.

geometric flexibility that allows nonplanar surface. Such flexibility is desired in practice but is difficult to achieve with purely analytical tools.

Unlike purely numerical tools, the new Esh3D does not require discretization of the inclusions. This is desirable if there are multiple and evolving inclusions. One can use the same mesh, as the inclusions are handled by the analytical part. To model evolving inclusion purely numerically, however, one needs to run an expensive mesh-remesh cycle. To model inclusions of extreme aspect ratios, a purely numerical tool may not be viable at all.

In many geophysical applications, I believe the benefit of this semi-analytical-numerical approach will outweigh the drawbacks. The new Esh3D still allows one to evaluate the full space solution without engaging the numerical part.

The new Esh3D evaluates the incomplete elliptical integrals with the Fukushima (2011) routine, replacing the Matlab routine. The code includes a custom Okada (1985) routine to allow multiple Eshelby's inclusions and Okada's faults in a single model. The Eshelby part will output both the full space and half-space solutions even if the half option is on. The new code, after all the improvements, remains openly available. Visit <https://github.com/Chunfang/Esh3D> for the latest updates and instructions.

2. Traction Cancellation to Obtain Half Space Solutions

In order to use the numerical routines, one needs to discretize the model domain with a finite element mesh. Figure 1 illustrates the traction cancellation scheme, which is implemented in several steps:

1. Run the analytical Eshelby's routines to evaluate displacement and stress at the centroids of the surface elements.

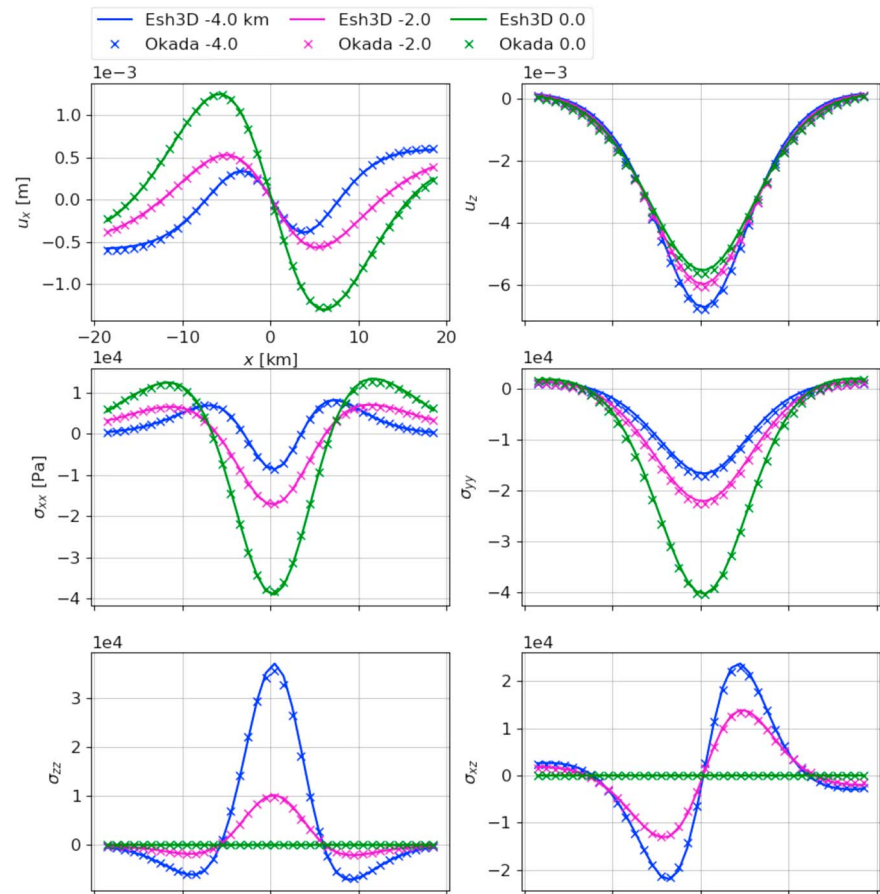


Figure 4. Displacement and stress above a $\pi/4$ dip-slip fault produced by Eshelby's inclusion and Okada's fault models.

2. Translate those stress tensors from the global coordinate (x, y, z) to the surface coordinate (x', y', z') , where the traction components $\sigma_{()z'}$ should be canceled.
3. Multiply the resulting traction by the element face areas to estimate the force that the empty side is acting on the elastic side.
4. Translate the force back to the global coordinate, and uniformly allocate a opposite force to the element's surface nodes.
5. Numerically solve this static loading problem, and superpose the numerical and analytical solutions to estimate the half-space solution.
6. Use the new stress tensors at the surface centroids to update the traction.
7. If the traction is not satisfyingly small, repeat this algorithm from the step 3 with the traction replaced by the remaining traction.

Being two linear systems, the Eshelby's perturbation and the strain by static loading can be superposed regardless of their temporal orders. The analytical part produces the objective traction over a continuous surface. The numerical part, on the other hand, implements the canceling traction via discrete nodal forces over a finite surface. This spatial mismatch requires this algorithm to seek the proper nodal forces that minimize the continuously varying traction in an iterative manner.

Because the numerical domain is finite, one has to apply roller boundary conditions to the sides and bottom. These boundaries only affect the numerical part of the solution, while the analytical part can have normal displacements at those boundaries. Although there are methods to emulate an infinite domain, for example, by having absorbing boundaries (Komatitsch & Tromp, 2003; Lysmer & Kuhlemeyer, 1969), but they are only applicable to dynamic problems. If one uses a dynamic model to implement the numerical part, the resulting surface traction will keep the infinite (half) domain moving permanently.

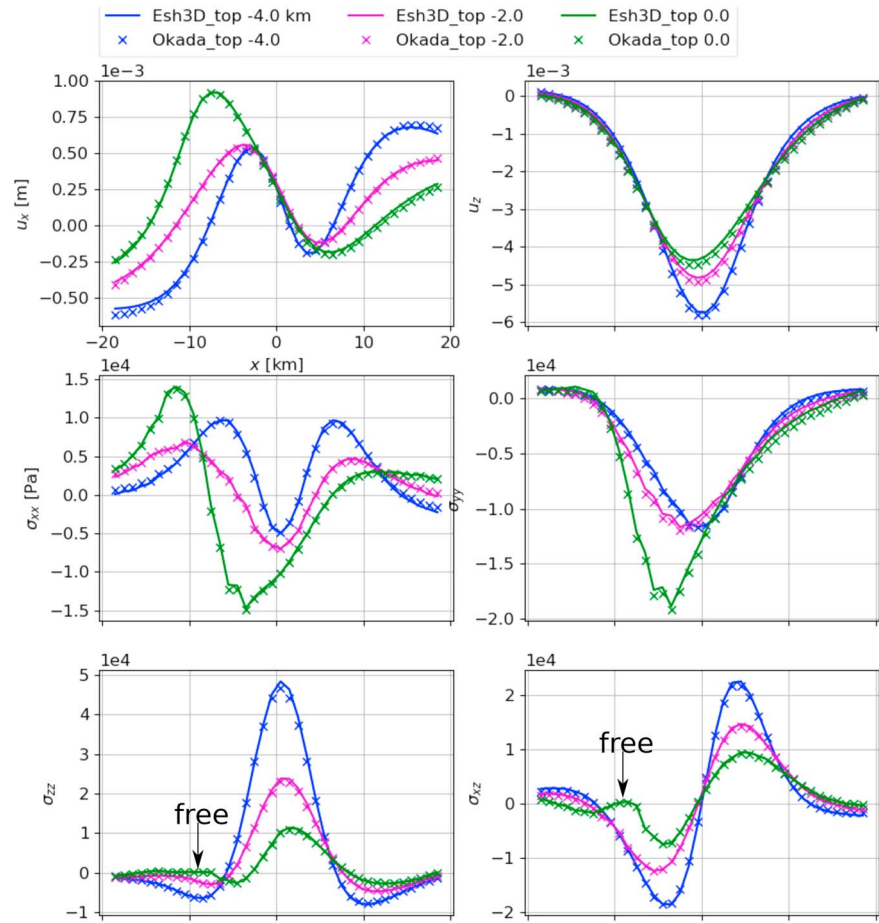


Figure 5. Displacement and stress above a $\pi/4$ dip-slip fault and below a nonplanar topography produced Eshelby's inclusion and Okada's fault models.

The numerical part in this study is derived from an open source finite element code Defmod, <https://bitbucket.org/stali/defmod>, introduced by Ali (2014). The domain truncation effect is discussed by Meng (2017, Appendix C).

3. Eshelby Versus Okada

Meng et al. (2012) validate the original code by transforming a triaxial inclusion to some simpler inclusion geometries for which the analytical solutions are known. In the same manner, I emulate a slipping fault and an opening fault with a low aspect (thin) ellipsoid under shear and tensile eigenstrains, respectively, and compare the solutions against the similar Okada solutions.

Table 1 lists the parameters for both the Eshelby's inclusion and Okada's fault. To make an equivalent Okada model, I overlay 60-by-40 Okada's tiles on the Eshelby's ellipsoid, as in Figure 2a. At each tile center, I multiply the interior Eshelby's strain with the local thickness of the ellipsoid to obtain the Okada's dislocation over the whole tile. In another word, I approximate the continuous motion around a low-aspect ellipsoid with piecewise uniform dislocations given by

$$\begin{aligned} \text{opening} &= h(i, j) \epsilon_{kk}, \\ \text{slip} &= h(i, j) (\epsilon_{ik} + \epsilon_{ki}), \end{aligned} \quad (7)$$

where $h(i, j)$ is the ellipsoid thickness in the k dimension at coordinate (i, j) .

I compare for two different dislocation modes, zero dip opening and $\pi/4$ dip slip, between the Eshelby's (inclusion/eigenstrain) model and the Okada's (fault/dislocation) model. Figure 2 (c and d) illustrates the numerical grids used for traction cancellation in cases of planar and topographical surfaces. The sides and

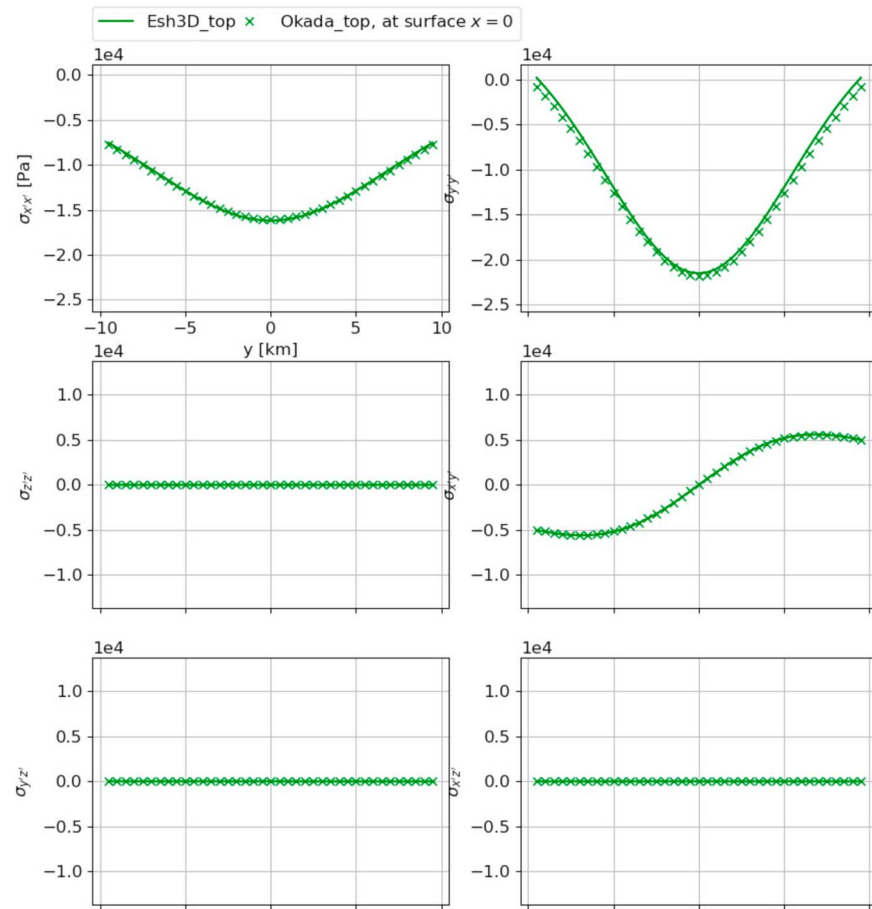


Figure 6. Local, (x', y', z') coordinate, stress at topographical surface above a $\pi/4$ dip-slip fault produced by Eshelby's inclusion and Okada's fault models.

bottom of the domain are given roller boundary conditions, i.e. no normal displacements are introduced by the numerical part. In the flat surface case, only the Eshelby solution requires traction cancellation, as the Okada solution is already for half-space.

3.1. Flat Surface

On the evaluation plane $y = 0$, the displacement component u_y and stress components σ_{xy} and σ_{yz} are zero due to symmetry. Therefore, I only compare the nonzero components in Figures 3 and 4. The opening mode fault models show noticeable disagreement in displacements, although having the stresses agreed. The dip-slip fault models show agreement in all comparisons. Two factors contribute to the disagreements especially in the opening mode case:

- The Okada's fault is a discretized approximation of the Eshelby's inclusion. The displacement and dislocation at the fault edge can never match; see Figure 2a.
- The inclusion follows volumetric laws, while the Okada's fault does not. The two solutions are similar when there is no volume change, for example, inclusion/fault under simple shear. When an inclusion elongates in one direction, it will shorten in the other orthogonal directions. The Okada's fault, in comparison, is not constrained by any laws. When the fault opens, its length stays unchanged.

This explains why the two models show greater disagreement in the opening mode case than in the dip-slip case.

In both the cases, the horizontal displacements, u_x , and the in-plane stress components, σ_{xx} and σ_{yy} , are amplified as the evaluation grid approaches the surface. The out-plane stress components, σ_{zz} and σ_{xz} , all reduce to 0 at $z = 0$, because they are equal to the normal and shear tractions, respectively.

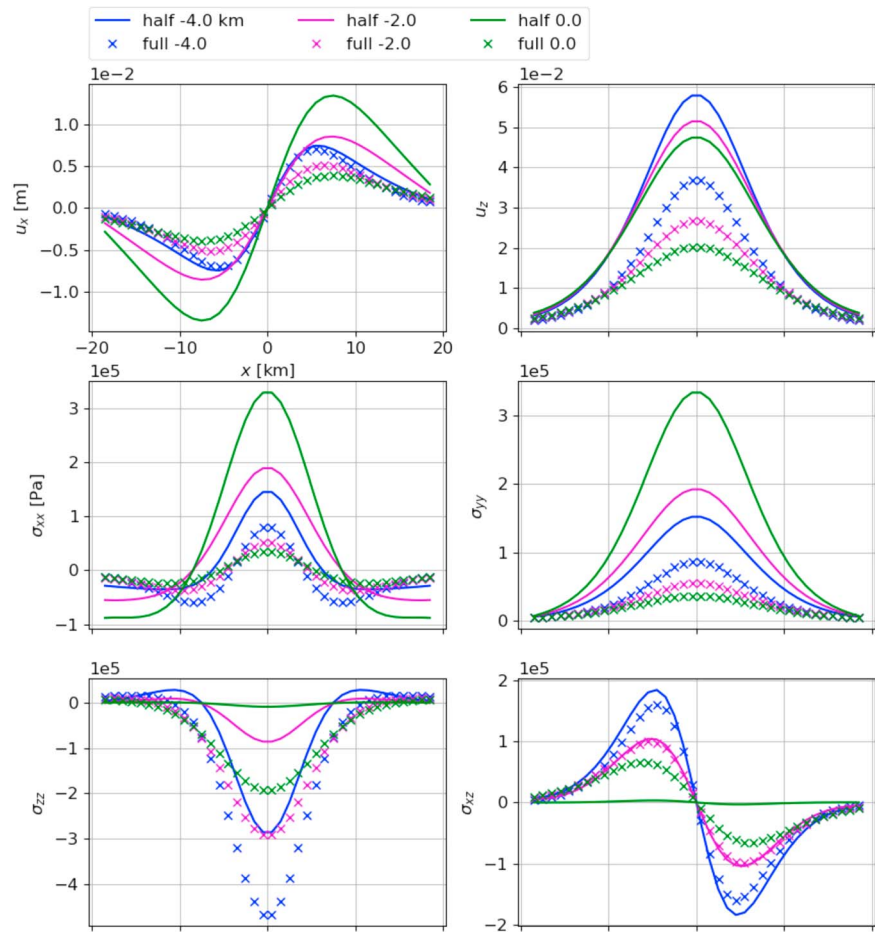


Figure 7. Displacement and stress comparisons between half-space and full space Eshelby solutions for uniaxial volume transformation within an ellipsoidal inclusion.

3.2. Topographical Surface

For the topographical case, illustrated by Figure 2d, I only compare the dip-slip solutions, because an Eshelby's inclusion is more equivalent to an Okada's fault in modeling slip mode fault than in modeling opening mode fault. Figure 5 compares the same nonzero quantities as in Figure 4.

The Eshelby and Okada solutions again show agreement, although the in-plane stress components σ_{xx} and σ_{yy} appear to suffer numerical artifacts. Because of the topography above, the out-plane stress components σ_{zz} and σ_{xz} at $z = 0$ are mostly nonzero, except at the tangential point, marked by “free” in Figure 2d, where the evaluation line meets the surface and the surface normal aligns with the z axis.

To better reveal the free surface, I translate the surface stress tensor from the global coordinate (x, y, z) to the local surface coordinate (x', y', z') , see Figure 1, and plot the six-component tensor along the line $x = 0$ in Figure 6. The three in-plane components, $\sigma_{x'x'}$, $\sigma_{y'y'}$, and $\sigma_{x'y'}$, are symmetric with respect to $y = 0$, because there is no topographical fluctuation in the y direction; see Figure 2d. The three traction components, $\sigma_{(-),z'}$, are all 0 as expected.

Note that, a custom Okada routine is included as a part of Esh3D such that Eshelby's inclusions and Okada's tiles can coexist in a single model. One can use Eshelby's inclusions to model volumetric objects and use Okada's tiles to model slipping fault patches. A benefit of this hybrid approach is that it allows Okada's faults beneath a topographical surface, which the original Okada code is incapable of.

4. Half Space Versus Full Space

To illustrate the free surface effect, I compare a half-space solution against corresponding full space solution. Figure 2b shows the inclusion model geometry and transformation. The elastic moduli and source location

are kept the same as in Table 1. Since here I compare two Eshelby solutions, I choose a volumetric ellipsoidal geometry of semiaxes (3, 2, 1) km, with a uniaxial eigenstrain $\epsilon_{kk} = 10^{-3}$, instead of the low-aspect geometry in the previous section.

Figure 7 compares the nonzero displacement and stress components resulting from the half-space and full space solutions. In contrast to the full space solution, the half-space solution has amplified displacement and in-plane stress components, while the out-plane stress components approach 0, when moving toward the surface. It is worth noticing that even at depth of 4 km, the free surface still has great impact to the displacement and stress.

5. Conclusion and Discussion

A traction cancellation approach in obtaining half-space Eshelby solution is implemented by an open source code Esh3D. A thin Eshelby's inclusion under simple shear is almost equivalent to corresponding Okada's fault. Due to the volumetric constraint that an inclusion is subject to, the thickening Eshelby's inclusion is noticeably different than the opening Okada's fault. Okada's fault is more flexible for modeling slipping fault patches, while Eshelby's inclusion is capable of modeling localized volume changes.

This semi-analytical-numerical approach allows one to model topographical surfaces. As a trade-off however, the results may be subject to numerical artifacts.

The free surface has significant impact to the displacement and stress fields above the Eshelby's inclusions. When moving toward the surface from below, the displacement and in-plane stress components are amplified, while the out-plane stress components approach zero.

Acknowledgments

This paper does not contain any measurement data. The Esh3D code is open source under MIT licence. Readers are encouraged to use and modify the code for their needs and cite this paper and (Meng et al., 2012) in their publications. To duplicate the results presented above, follow the instructions at GitHub website (<https://github.com/Chunfang/Esh3D>). The author was supported by ExxonMobil via MIT Energy Initiative Project (MITe) Founding Member Agreement 10/1/14. This work used the Extreme Science and Engineering Discovery Environment (XSEDE) Bridges computer at PSC through allocation TG-GEO170009, which is supported by National Science Foundation grant ACI-1548562. The author thanks Dazhi Jiang and John Rudnicki for their thoughtful and detailed reviews.

References

- Ali, S. T. (2014). Defmod—Parallel multiphysics finite element code for modeling crustal deformation during the earthquake/rifting cycle. arXiv:1402.0429, <http://arxiv.org/abs/1402.0429>
- Bedayat, H., & Dahi Taleghani, A. (2015). Pressurized poroelastic inclusions: Short-term and long-term asymptotic solutions. *Rock Mechanics and Rock Engineering*, 48(6), 2359–2367. <https://doi.org/10.1007/s00603-014-0705-7>
- Carter, S. T., Rotella, J., Agyei, R. F., Xiao, X., & Sangid, M. D. (2018). Measuring fatigue crack deflections via cracking of constituent particles in AA7050 via in situ X-ray synchrotron-based micro-tomography. *International Journal of Fatigue*, 116, 490–504. <https://doi.org/10.1016/j.ijfatigue.2018.07.005>
- Eidelman, A., & Reches, Z. (1992). Fractured pebbles—A new stress indicator. *Geology*, 20(4), 307–310. [https://doi.org/10.1130/0091-7613\(1992\)020<0307:FPANSI>2.3.CO;2](https://doi.org/10.1130/0091-7613(1992)020<0307:FPANSI>2.3.CO;2)
- Eshelby, J. D. (1957). The determination of the elastic field of an ellipsoidal inclusion, and related problems. *Proceedings of the Royal Society of London. Series A. Mathematical and Physical Sciences*, 241(1226), 376–396. <https://doi.org/10.1098/rspa.1957.0133>
- Eshelby, J. D. (1959). The elastic field outside an ellipsoidal inclusion. *Proceedings of the Royal Society of London. Series A. Mathematical and Physical Sciences*, 252(1271), 561–569. <https://doi.org/10.1098/rspa.1959.0173>
- Eshelby, J. D. (1961). Elastic inclusion and inhomogeneities. *Progress in Solid Mechanics*, 2, 89–140.
- Ferrers, N. M. (1877). On the potentials of ellipsoids, ellipsoidal shells, elliptic laminae and elliptic rings of variable densities. *The Quarterly Journal of Pure and Applied Mathematics*, 14, 1–22.
- Fukushima, T. (2011). Precise and fast computation of a general incomplete elliptic integral of second kind by half and double argument transformations. *Journal of Computational and Applied Mathematics*, 235(14), 4140–4148. <https://doi.org/10.1016/j.cam.2011.03.004>
- Gradshteyn, I., & Ryzhik, I. (1965). *Table of integrals, series, and products*. New York: Academic Press.
- Guido, F. L., Antonellini, M., & Picotti, V. (2015). Modeling ground displacement above reservoirs undergoing fluid withdrawal/injection based on an ellipsoidal inhomogeneity mode. *International Journal of Rock Mechanics and Mining Sciences*, 79, 63–69. <https://doi.org/10.1016/j.ijrmms.2015.08.010>
- Healy, D. (2009). Short note: Elastic field in 3D due to a spheroidal inclusion—MATLAB code for Eshelby's solution. *Computers & Geosciences*, 35, 2170–2173. <https://doi.org/10.1016/j.cageo.2008.11.012>
- Healy, D., Jones, R. R., & Holdsworth, R. E. (2006). Three-dimensional brittle shear fracturing by tensile crack interaction. *Nature*, 439(7072), 64–67. <https://doi.org/10.1038/nature04346>
- Igor, M. (2005). Elliptic integrals and functions. Math Work.
- Jiang, D. (2007). Numerical modeling of the motion of deformable ellipsoidal objects in slow viscous flows. *Journal of Structural Geology*, 29(3), 435–452. <https://doi.org/10.1016/j.jsg.2006.09.009>
- Jiang, D. (2014). Structural geology meets micromechanics: A self-consistent model for the multiscale deformation and fabric development in Earth's ductile lithosphere. *Journal of Structural Geology*, 68, 247–272. <https://doi.org/10.1016/j.jsg.2014.05.020>
- Jiang, D. (2016). Viscous inclusions in anisotropic materials: Theoretical development and perspective applications. *Tectonophysics*, 693, 116–142. <https://doi.org/10.1016/j.tecto.2016.10.012>
- Ju, J., & Sun, L. (1999). Novel formulation for the exterior-point Eshelby's tensor of an ellipsoidal inclusion. *Journal of Applied Mechanics*, 66(2), 570–574. <https://doi.org/10.1115/1.2791090>
- Katsman, R. (2010). Extensional veins induced by self-similar dissolution at stylolites: Analytical modeling. *Earth and Planetary Science Letters*, 299(1–2), 33–41. <https://doi.org/10.1016/j.epsl.2010.08.009>
- Komatitsch, D., & Tromp, J. (2003). A perfectly matched layer absorbing boundary condition for the second-order seismic wave equation. *Geophysical Journal International*, 154(1), 146–153. <https://doi.org/10.1046/j.1365-246X.2003.01950.x>
- Lysmer, J., & Kuhlemeyer, R. L. (1969). Finite dynamic model for infinite media. *Journal of Engineering Mechanics-ASCE*, 859, 877.

- Meng, C. (2017). Benchmarking Defmod, an open source FEM code for modeling episodic fault rupture. *Computers and Geosciences*, 100, 10–26. <https://doi.org/10.1016/j.cageo.2016.11.014>
- Meng, C., Heltsley, W., & Pollard, D. D. (2012). Evaluation of the Eshelby solution for the ellipsoidal inclusion and heterogeneity. *Computers and Geosciences*, 40, 40–48. <https://doi.org/10.1016/j.cageo.2011.07.008>
- Meng, C., Maerten, F., & Pollard, D. D. (2013). Modeling mixed-mode fracture propagation in isotropic elastic three dimensional solid. *International Journal of Fracture*, 179(1), 45–57. <https://doi.org/10.1007/s10704-012-9771-6>
- Meng, C., & Pollard, D. D. (2014). Eshelby's solution for ellipsoidal inhomogeneous inclusions with applications to compaction bands. *Journal of Structural Geology*, 67, 1–19. <https://doi.org/10.1016/j.jsg.2014.07.002>
- Mura, T. (1987). *Micromechanics of defects in solids*. Dordrecht, Netherlands: Kluwer Academic Pub.
- Niu, Z., Li, Q., & Wei, X. (2017). Estimation of the surface uplift due to fluid injection into a reservoir with a clayey interbed. *Computers and Geotechnics*, 87, 198–211. <https://doi.org/10.1016/j.compgeo.2017.02.015>
- Okada, Y. (1985). Surface deformation to shear and tensile faults in a halfspace. *Bulletin of the Seismological Society of America*, 75, 1135–1154.
- Reches, Z. (1998). Tensile fracturing of stiff rock layers under triaxial compressive stress states. *International Journal of Rock Mechanics and Mining Sciences*, 35(4-5), 70.
- Rudnicki, J. W. (1977). The inception of faulting in a rock mass with a weakened zone. *Journal of Geophysical Research*, 82(5), 844–854. <https://doi.org/10.1029/JB082i005p00844>
- Rudnicki, J. W. (1999). Alteration of regional stress by reservoirs and other inhomogeneities: Stabilizing or destabilizing? *International Society for Rock Mechanics and Rock Engineering*, 3, 1629–1637.
- Sharma, P., & Ganti, S. (2004). Size-dependent Eshelby's tensor for embedded nano-inclusions incorporating surface/interface energies. *Journal of Applied Mechanics*, 71(5), 663–671. <https://doi.org/10.1115/1.1781177>
- Svoboda, J., Ecker, W., Razumovskiy, V., Zickler, G., & Fischer, F. (2018). Kinetics of interaction of impurity interstitials with dislocations revisited. *Progress in Materials Science*. <https://doi.org/10.1016/j.pmatsci.2018.10.001>
- Townsend, M., Pollard, D. D., Johnson, K., & Culha, C. (2015). Jointing around magmatic dikes as a precursor to the development of volcanic plugs. *Bulletin of Volcanology*, 77(10), 92. <https://doi.org/10.1007/s00445-015-0978-z>